



Identification of 2-amino-5-aryl-pyrazines as inhibitors of human lactate dehydrogenase



Benjamin P. Fauber^{a,*}, Peter S. Dragovich^a, Jinhua Chen^b, Laura B. Corson^a, Charles Z. Ding^b, Charles Eigenbrot^a, Anthony M. Giannetti^a, Thomas Hunsaker^a, Sharada Labadie^a, Yichin Liu^a, Yingchun Liu^b, Shiva Malek^a, David Peterson^a, Keith Pitts^a, Steve Sideris^a, Mark Ultsch^a, Erica VanderPorten^a, Jing Wang^b, BinQing Wei^a, Ivana Yen^a, Qin Yue^a

^a Genentech, Inc., 1 DNA Way, South San Francisco, CA 94080, USA

^b WuXi AppTec Co., Ltd, 288 Fute Zhong Road, Waigaoqiao Free Trade Zone, Shanghai 200131, PR China

ARTICLE INFO

Article history:

Received 9 July 2013

Revised 9 August 2013

Accepted 13 August 2013

Available online 22 August 2013

Keywords:

Lactate dehydrogenase

X-ray crystal structure

Pyrazine

Tumor metabolism

ABSTRACT

A 2-amino-5-aryl-pyrazine was identified as an inhibitor of human lactate dehydrogenase A (LDHA) via a biochemical screening campaign. Biochemical and biophysical experiments demonstrated that the compound specifically interacted with human LDHA. Structural variation of the screening hit resulted in improvements in LDHA biochemical inhibition and pharmacokinetic properties. A crystal structure of an improved compound bound to human LDHA was also obtained and it explained many of the observed structure–activity relationships.

© 2013 Elsevier Ltd. All rights reserved.

Since the early 20th century, it has been known that many tumors exhibit altered metabolic characteristics relative to normal tissues.¹ One of the major differences between cancerous and normal tissues is how they metabolize glucose. Some cancer cells primarily metabolize glucose by glycolysis, whereas most normal cells catabolize glucose by oxidative phosphorylation.² Such differences in normal and tumor cell metabolism represent attractive therapeutic opportunities to selectively target tumor cells.³

The shift toward anaerobic glycolysis with a concomitant increase in lactate production is a hallmark of rapidly-proliferating cells (known as the Warburg Effect).⁴ The conversion of both glucose and glutamine to lactate under anaerobic conditions involves the enzyme lactate dehydrogenase A (LDHA). It has been known for several decades that LDHA is over-expressed in human tumor tissue.⁵ Additionally, shRNA knockdown of LDHA expression in tumor cell lines elicited a decrease in cell proliferation under hypoxic conditions.⁶ These observations, coupled with viability of human genetic knock-outs, make LDHA an attractive target for inhibiting tumor cell proliferation.^{7,8}

Some inhibitors of human LDHA have been reported in the literature.^{9–13} The most potent and well-characterized of these inhibitors resulted from fragment screening campaigns.^{10,11}

Biochemical screening efforts at Genentech identified a series of 2-thio-6-oxo-1,6-dihydropyrimidines, which we disclosed in an earlier publication (Fig. 1, compound 1).¹⁴ We now describe the identification, validation, and structure–activity relationships of an amino-pyrazine biochemical screening hit from the Genentech/Roche corporate compound collection (Fig. 1, compound 2).

Compound 2 was identified using a human LDHA biochemical assay that monitored the disappearance of the NADH co-factor during enzymatic conversion of pyruvate to lactate ($IC_{50} = 4 \mu M$).^{15,16} Compound 2 also demonstrated a favorable ligand-efficiency (LE) value in our LDHA biochemical assay ($LE = 0.30$).¹⁷ Importantly, a similar IC_{50} value was achieved when LDHA biochemical inhibition was quantified using mass spectrometry, suggesting that the observed biochemical inhibition did not result from spectrophotometric assay artifacts. Biochemical assay using structurally-related human lactate dehydrogenase B (LDHB) also demonstrated a similar biochemical potency ($IC_{50} = 12 \mu M$).¹⁸

In addition to biochemical assays, compound 2 was profiled using a surface plasmon resonance (SPR) assay.¹⁶ Analysis of human LDHA and compound 2 in the absence of NADH provided a very weak SPR K_D value ($K_D = 857 \mu M$). In comparison, compound 2 associated with LDHA in the presence of NADH and with a K_D that closely matched the biochemical IC_{50} value ($K_D = 7 \mu M$). These differing SPR binding results illustrated the cooperative binding of the NADH co-factor and compound 2 in a manner that might parallel

* Corresponding author.

E-mail address: benjampf@gene.com (B.P. Fauber).

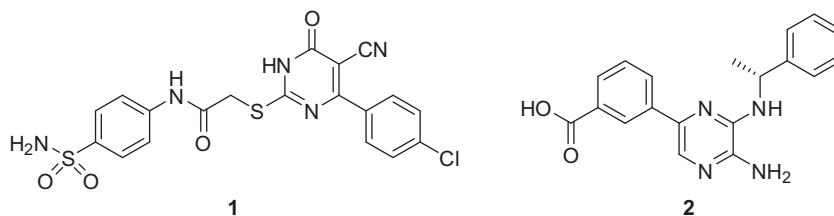


Figure 1. LDHA inhibitors identified via biochemical screening campaigns at Genentech.

events occurring during the catalytic conversion of pyruvate to lactate.¹⁹ Taken collectively, these biochemical and biophysical results suggested that compound **2** was a validated human lactate dehydrogenase inhibitor worthy of additional investigation.

It was recognized that the carboxylic acid motif present in compound **2** could result in poor in vivo pharmacokinetics due to phase II metabolism of the acid moiety.²⁰ Thus, structural exploration commenced with modification of the 5-position of the 2-amino-pyrazine core in an effort to explore carboxylic acid replacements while maintaining favorable potency (Table 1). Replacement of the aryl carboxylic acid with an aryl ester eroded activity, as did replacement of the carboxylic acid with an amide or acyl-sulfonamide group (Table 1, compounds **3–5**, respectively). Use of a 3-carboxy-4-pyridyl ring resulted in some loss of potency (Table 1, compound **6**). Optimal placement of the carboxylic acid group was probed by moving it to the 2-position of the arene, which was not tolerated (Table 1, compound **7**), whereas movement of the acid group to the 4-position of the arene resulted in only a modest reduction in potency (Table 1, compound **8**). Introduction of a 3-phenol adjacent to the 4-carboxylic acid to facilitate an intramolecular hydrogen bond between the groups, and thus limit rotation about the carbonyl–aryl C–C bond and make it co-planar with the aromatic ring, did not provide a significant improvement in potency versus the parent 4-carboxylic acid analog (Table 1, compounds **9** and **8**, respectively). Conversion of the arene to a 4-carboxy-*N*-pyrazole retained potency, while conversion to a carboxy-thiophene displayed less biochemical activity (Table 1, compounds **10** and **11**, respectively).

After analyzing the analogs in Table 1, it was clear that the acidic functionality present in compound **2** was preferred. A similar preference has also been noted in other LDHA inhibitors.^{9–13} The aforementioned SAR preferences were subsequently explained by the crystallographic observation that the carboxylic acid group makes a hydrogen bond interaction with a histidine residue in the LDHA binding pocket (see below).

The next phase of exploration focused on substitution of the 3-benzoic acid ring while maintaining the important acidic functionality. Systematic exploration of the 2-, 4-, 5-, and 6-positions of the ring are detailed in Table 2. Methylation of the various positions about the ring indicated a preference for the 6-position (Table 2, compounds **12–15**). Additional 6-position groups were explored, including the larger *iso*-propyl group, as well as electron-donating and electron-withdrawing groups (Table 2, compounds **16–18**). All 6-position changes had minimal impact on the potencies of the molecules, indicating a steric preference for substitution at the 6-position of the aryl ring with minimal substituent-induced electronic effects. The 6-position group was subsequently shown by crystallography to make a lipophilic interaction with the protein pocket, explaining the preference for the 6-position over the other locations on the aromatic ring (see below). Additionally, the disfavored substitution at the 2- and 4-positions of the ring could be rationalized as disrupting the bond angle between the carboxylic acid and the arene. These bond angle disruptions could in turn

upset the aforementioned carboxylic acid group's interaction with the histidine residue in the LDHA binding pocket.

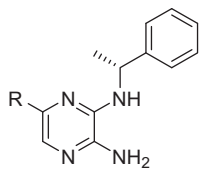
We then turned our attention to exploration of the (*R*)-methyl-benzyl amine region of the molecule. Removal of the chiral α -methyl group resulted in a slight loss of potency, while the (*S*)-methyl-benzyl amine produced an inactive molecule (Table 3, compounds **19** and **20**, respectively). A rationalization for the loss in potency was subsequently explained by the crystallographic observation that the benzylic group fills a hydrophobic region of the pocket where there is limited space to accommodate the opposite torsional orientation of the benzylic group that would be induced by the (*S*)-enantiomer (see below).

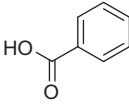
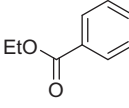
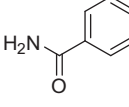
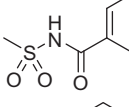
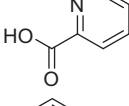
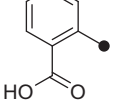
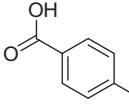
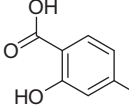
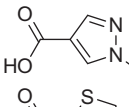
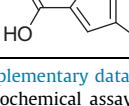
We explored chlorine substitution on the phenyl ring of the (*R*)-methyl-benzyl amine and found the 4-chloro-group provided an approximate twofold improvement in potency (Table 3, compound **21**). Methylation of the N–H moiety resulted in an inactive molecule, as did replacement of the secondary amine with an ether linkage to the pyrazine core (Table 3, compounds **22** and **23**, respectively). Taken collectively, these data points suggested a strict steric requirement for the positioning of the benzylic group. Saturation of the benzylic ring, along with inclusion of another saturated ring analog, was tolerated (Table 3, compounds **24** and **25**). However, an amino-ether analog was not permitted, indicating a preference for lipophilic groups in this region of the binding site (Table 3, compound **26**).

Having explored the peripheral regions of the 2-amino-pyrazine hit, we then focused our effort on the pyrazine core present in **2**. Single-point changes were conducted to understand the contributions of each core element to the overall potency of the molecule. Systematic removal of the pyrazine ring nitrogens indicated a requirement for the 1-position nitrogen (Table 4, compounds **27** and **28**). Removal of the 2-amino group, or conversion to a 2-phenol group, resulted in a loss of potency (Table 4, compounds **29** and **30**).²¹ Likewise, further changes to the 2-amino position including methylation, acylation, and sulfonylation of the amino-group were not tolerated (Table 4, compounds **31–33**). Inclusion of a 6-methyl-group on the 2-amino-pyrazine core resulted in a loss of potency (Table 4, compound **34**). Taken collectively, these data points indicated a strong binding site preference for the hydrogen bond donor–acceptor motif present in the 2-amino-pyrazine scaffold.

To further explain the observed SAR in this series, we obtained a 2.05 Å resolution crystal structure of an improved inhibitor bound to human LDHA in the presence of NADH.²² As shown in Figure 2a, compound **18** binds near several conserved residues involved in the catalytic processing of lactate dehydrogenase substrates (i.e., Arg168 and His192).²³ The NADH co-factor was also observed in the crystal structure, adjacent to compound **18** and in a configuration similar to that previously described in the literature.²⁴ The hydrogen bonding interactions of compound **18** are summarized in Figure 2b. The compound formed a hydrogen bond via its carboxylic acid group to His192, but did not interact with Arg168 (>5 Å distance). This interaction was consistent with the requirement for the carboxylic acid group on the 3-position ring (Table 1).

Table 1
Structure–activity relationships of the 5-position of the 2-amino-pyrazine



Compd	R-group	LDHA IC ₅₀ ^a (μM)	LDHA SPR K _D ^b (μM)	LDHB IC ₅₀ ^c (μM)	LDHA LE ^d
2		4	7	12	0.30
3		>100	>100	ND	–
4		>100	>100	92	–
5		>100	>100	>100	–
6		24	32	48	0.26
7		>100	>100	>100	–
8		14	ND	16	0.27
9		10	ND	16	0.27
10		15	ND	15	0.28
11		50	33	>100	0.25

See the [Supplementary data](#) for experimental details associated with each assessment. All biochemical assay results are reported as the arithmetic mean of two separate runs ($n = 2$). SPR data are $n = 1$. ND = not determined.

^a Human LDHA biochemical inhibition.¹⁵

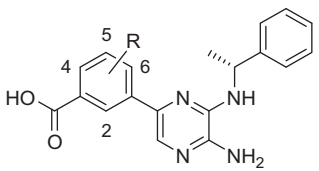
^b Human LDHA dissociation constant as determined by surface plasmon resonance (SPR).

^c Human LDHB biochemical inhibition.

^d Ligand efficiency (LE) was calculated using the human LDHA biochemical IC₅₀ value.¹⁷

In addition to interacting with His192, compound **18** also formed a hydrogen bond between the N–H of the 3-(*R*)-methyl-benzylamine group and the α -phosphate oxygen of the NADH co-factor. This crystallographic ligand interaction with the NADH co-factor was consistent with the SPR result discussed earlier in which a related compound exhibited a much higher affinity for LDHA in the

Table 2
Structure–activity relationships of the benzoic-acid region of the 2-amino-pyrazine



Compd	R-group	LDHA IC ₅₀ ^a (μM)	LDHA SPR K _D ^b (μM)	LDHB IC ₅₀ ^c (μM)	LDHA LE ^d
12	2-Me	35	>100	44	0.24
13	4-Me	15	29	40	0.26
14	5-Me	4	7	7	0.29
15	6-Me	2	3	6	0.31
16	6- ^t Pr	2	5	7	0.29
17	6-OMe	2	3	7	0.29
18	6-Cl	2	5	8	0.31

See the [Supplementary data](#) for experimental details associated with each assessment. All biochemical assay results are reported as the arithmetic mean of two separate runs ($n = 2$). SPR data are $n = 1$. ND = not determined.

^a Human LDHA biochemical inhibition.¹⁵

^b Human LDHA dissociation constant as determined by surface plasmon resonance (SPR).

^c Human LDHB biochemical inhibition.

^d Ligand efficiency (LE) was calculated using the human LDHA biochemical IC₅₀ value.¹⁷

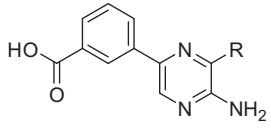
presence of the co-factor. Additionally, this interaction also explained the loss of affinity described earlier in this work that resulted from the conversion of the benzylic N–H linker into a benzylic ether linkage. The ether linkage would have created a repulsing lone-pair lone-pair effect between the ether oxygen and the α -phosphate oxygen of NADH.

A hydrogen bond acceptor–donor interaction motif between Thr247 and the 2-amino-pyrazine core of compound **18** was also observed. This observation was consistent with the strict SAR requirements we noted in our core change analogs that systematically disrupted the acceptor–donor motif ([Table 4](#)). Compound **18** did not make any detectable interactions with water molecules in the binding site.

The 6-chloro-group on the benzoic acid ring and the 3-(*R*)-methyl-benzylamine group formed a hydrophobic interaction with Ile241 in the binding site ([Fig. 2a](#)). Again, these structural observations were consistent with the previously discussed SAR studies and stereochemical requirements at the 3-position of the pyrazine core ([Table 3](#)). The (*R*)-methyl-benzylamine group made several close contacts with the surrounding protein residues. This binding mode was consistent with the observation that the (*S*)-methyl analog was detrimental to potency, presumably due to a lack of space to accommodate other rotational orientations of the benzylic group induced by the (*S*)-enantiomer.

In an effort to combine preferred fragments identified by the above activities into one molecule, we synthesized a 6-methyl-3-benzoic acid analog bearing a 4-chloro-(*R*)-methyl-benzylamine ([Fig. 3](#), compound **35**). The combination of these features resulted in a human LDHA inhibition IC₅₀ of 0.50 μM. Additionally, compound **35** was fourfold selective versus human LDHB, 10-fold selective versus human lactate dehydrogenase C (LDHC), and >500-fold selective versus the structurally-related human malate dehydrogenase 1 (MDH1) and human malate dehydrogenase 2 (MDH2) enzymes.²⁵ compound **35** was not profiled against a kinase selectivity panel, but it is anticipated that it could possess some kinase binding affinity due to its hydrogen bond donor–acceptor motif (i.e., 2-amino-pyrazine) commonly found in kinase inhibitors.²⁶

Table 3
Structure–activity relationships of the 3-position of the 2-amino-pyrazine



Compd	R-group	LDHA IC ₅₀ ^a (μM)	LDHA SPR K _D ^b (μM)	LDHB IC ₅₀ ^c (μM)	LDHA LE ^d
19		12	22	28	0.29
20		>100	>100	ND	—
21		2	5	5	0.31
22		>100	>100	ND	—
23		>100	>100	>100	—
24		3	7	16	0.31
25		19	18	80	0.29
26		>100	>100	ND	—

See the [Supplementary data](#) for experimental details associated with each assessment. All biochemical assay results are reported as the arithmetic mean of two separate runs ($n = 2$). SPR data are $n = 1$. ND = not determined.

^a Human LDHA biochemical inhibition.¹⁵

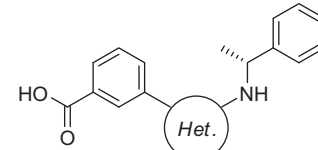
^b Human LDHA dissociation constant as determined by surface plasmon resonance (SPR).

^c Human LDHB biochemical inhibition.

^d Ligand efficiency (LE) was calculated using the human LDHA biochemical IC₅₀ value.¹⁷

Compounds **2** and **35** were profiled against a panel of in vitro DMPK assays. In addition to compound **35** being a more potent inhibitor of LDHA than compound **2**, there were also improvements in the liver microsomal stabilities in humans and rats ([Table 5](#)). Both compounds also exhibited favorable aqueous kinetic solubility and cell permeability in the Madin–Darby canine kidney (MDCK) cell permeability model.²⁷ Additionally, neither compound inhibited the major cytochrome P450 (CYP) isoforms up to compound concentrations of 10 μM.²⁸ Compound **35** was profiled in an in vivo single-dose rat pharmacokinetic experiment (1.5 mg/kg po and 0.5 mg/kg iv) and demonstrated high in vivo clearance (Cl_p = 60 mL/min/kg), a modest volume of distribution (V_d = 1.4 L/

Table 4
Structure–activity relationships of the 2-amino-pyrazine core



Compd	Heterocycle	LDHA IC ₅₀ ^a (μM)	LDHASPR K _D ^b (μM)	LDHB IC ₅₀ ^c (μM)	LDHA LE ^d
27 ^e		18	29	56	0.27
28		>100	>100	ND	—
29		25	>100	23	0.27
30 ²¹		>100	>100	>100	—
31		73	>100	>100	0.22
32		>100	ND	>100	—
33		71	ND	>100	0.20
34		91	>100	>100	0.22

See the [Supplementary data](#) for experimental details associated with each assessment. All biochemical assay results are reported as the arithmetic mean of two separate runs ($n = 2$). SPR data are $n = 1$. ND = not determined.

^a Human LDHA biochemical inhibition.¹⁵

^b Human LDHA dissociation constant as determined by surface plasmon resonance (SPR).

^c Human LDHB biochemical inhibition.

^d Ligand efficiency (LE) was calculated using the human LDHA biochemical IC₅₀ value.¹⁷

kg), and 41% oral availability in male Sprague–Dawley rats ([Table 6](#)).

We also assessed the ability of compound **35** to inhibit the production of lactate in MCF7 cells.¹⁶ No dose–response was observed in the assay but at the highest compound concentration of 50 μM, we observed a 40% reduction in lactate production with no effect on cell viability. The reasons for the minimal cellular activity are currently unknown, but could be related to insufficient biochemical potency or high plasma–protein binding (>99% bound in human plasma and 99% bound in rodent plasma). Additional experiments are ongoing to clarify which, if any, of these potential liabilities is responsible for the poor cell-based activity exhibited by compound **35**.

Syntheses of analogs that explored the 3- and 5-positions of the 2-amino-pyrazine core are described in [Scheme 1](#). The route com-

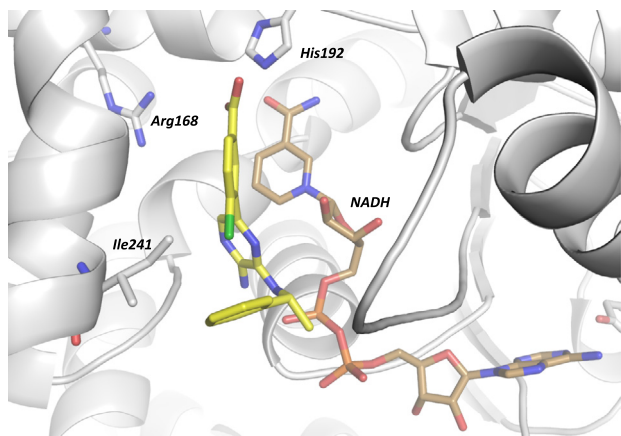


Figure 2a. Co-crystal structure of compound **18** (yellow) in complex with LDHA (grey). NADH is also present (gold). Nearby side-chain residues involved in the catalytic processing of lactate dehydrogenase substrates are also shown in grey (Arg168 and His192). Ile241 (grey) makes a hydrophobic contact with compound **18**. Compound **18** does not make any direct interactions with water molecules, thus they have been omitted for clarity. Hydrogen bonds are not depicted in this figure. The resolution of the structure is 2.05 Å.

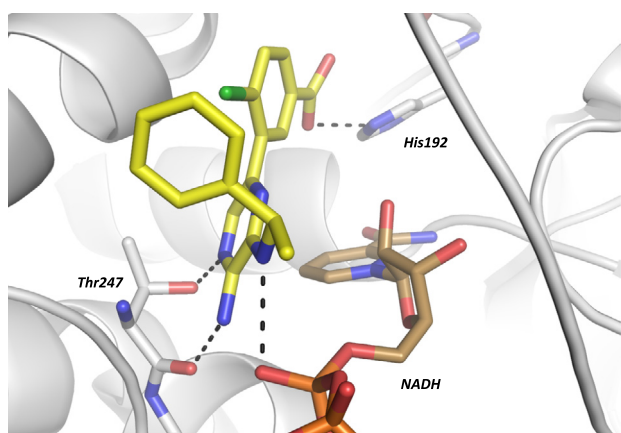


Figure 2b. Alternate view of co-crystal structure of compound **18** (yellow) in complex with LDHA (grey). NADH is also present (gold). Hydrogen bonds are depicted as dashed lines (black), with distances ranging from 2.9 to 3.1 Å.

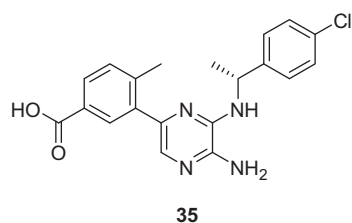


Figure 3. Combination of the most potent structural features in one molecule.

Table 5
In vitro DMPK properties of compounds **2** and **35**

Compd	HLM ^a Cl _{hep} (mL/min/kg)	RLM ^b Cl _{hep} (mL/min/kg)	Human/rat plasma-protein binding (% bound)	MDCK permeability ^c A–B (10 ^{−6} cm/s)	MDCK permeability ^c B–A (10 ^{−6} cm/s)	Solubility ^d (μM)
2	5	9	99/96	9.6	4.0	137
35	1	4	>99/99	12.1	10.3	81

See the [Supplementary data](#) for experimental details associated with each assessment.

^a Human in vivo clearance value extrapolated from in vitro human liver microsome (HLM) experiment.

^b Rat in vivo clearance value extrapolated from in vitro rat liver microsome (RLM) experiment.

^c Madin–Darby canine kidney (MDCK) cell permeability assay to assess membrane permeability properties.²⁷

^d Aqueous kinetic solubility at pH 7.4 (estimated from a high-throughput assay).

Table 6
Single-dose rat in vivo pharmacokinetic properties of compound **35**

Compd	Cl _p (mL/min/kg)	V _d (L/kg)	C _{max(iv)} (μM)	AUC _{inf(po)} (h μM)	t _{1/2} (h)	% F ^b
35 ^a	60	1.4	2.1	0.55	2.8	41

See the [Supplementary data](#) for experimental details associated with each assessment. Data reported are the arithmetic means from the dosing cohorts.

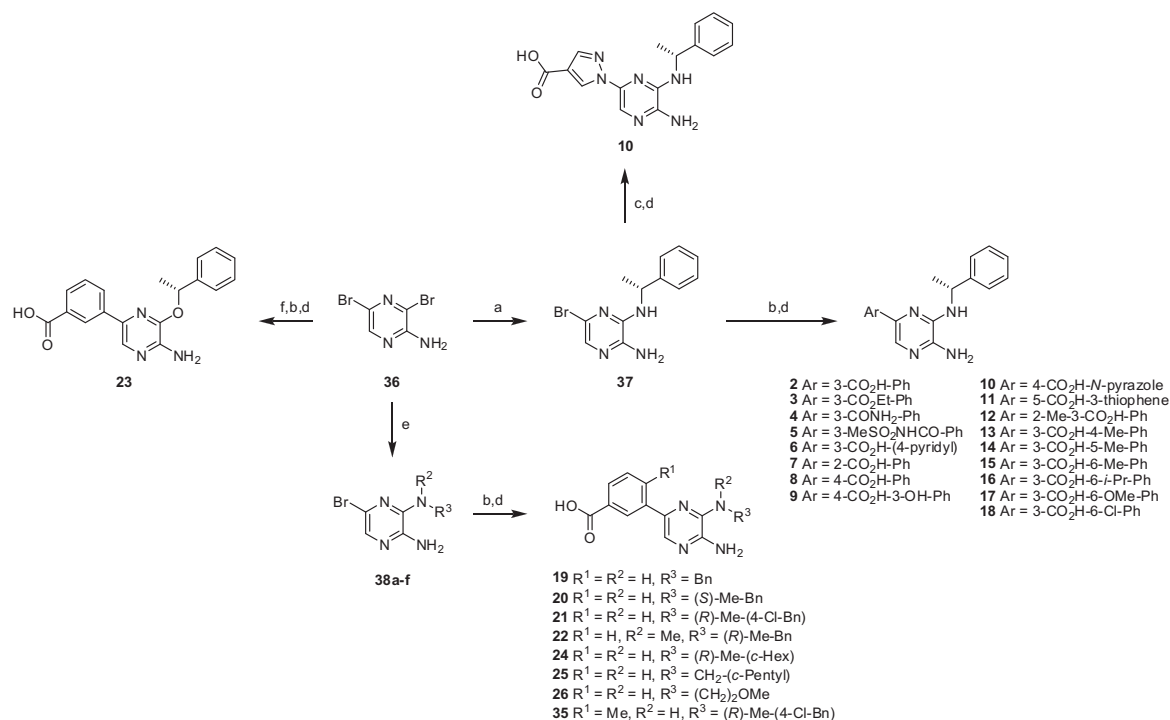
^a Male Sprague–Dawley rats (*n* = 3), 1.5 mg/kg po (26/74 suspension of DMSO/MCT), 0.5 mg/kg iv (18/60/22 solution of DMSO/PEG400/saline).

^b Bioavailability was calculated according to the equation % F = (AUC_{po} × Dose_{iv}/AUC_{iv} × Dose_{po}) × 100.

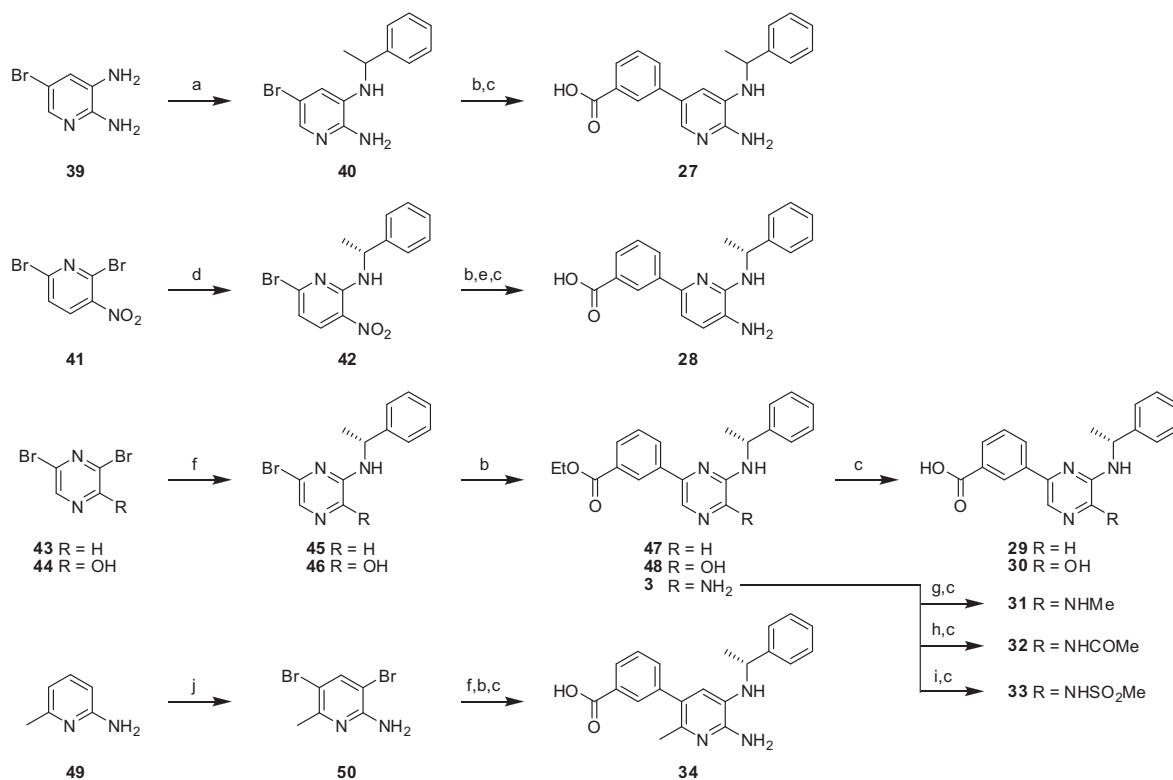
menced with the S_NAr reaction of various amines on the 3,5-dibromo-2-amino-pyrazine scaffold ([Scheme 1](#), Intermediate **36**).²⁹ The pyrazine–aryl bond was formed under Suzuki–Miyaura cross-coupling conditions, or Buchwald–Hartwig amination conditions for analogs that contained a pyrazine-*N*-heteroaryl bond.^{30,31} Final compounds containing a carboxylic acid were carried through the synthetic sequences as the corresponding ethyl ester, then saponified in the final step to reveal the carboxylic acid ([Scheme 1](#), compounds **2–18**).

Changes to the pyrazine core are summarized in [Scheme 2](#). Pyridine compound **27** was made from the alkylation of 5-bromopyridine-2,3-diamine with (1-bromoethane)benzene to yield the corresponding racemic product ([Scheme 2](#), compound **40**).³² A Suzuki–Miyaura coupling of the remaining halide, followed by saponification provided the final compound (**27**). The pyridine isomer of the aforementioned analog was synthesized via a S_NAr reaction with (*R*)-methyl-benzylamine to produce intermediate **42**,³³ followed by a Suzuki–Miyaura coupling. Subsequent reduction of the nitro-group and saponification of the ester revealed pyridine compound **28**. Compounds **29** and **30** were made using varied starting materials and a similar procedure as described in [Scheme 1](#). Compound **3** was further elaborated into the *N*-methyl analog using reductive methylation, as well as *N*-acetyl and *N*-sulfonyl analogs under standard conditions, followed by saponification to reveal the final compounds ([Scheme 2](#), compounds **31–33**). The 2-amino-6-methylpyrazine core was generated via the dibromination of 2-amino-6-methylpyrazine,³⁴ followed by a S_NAr reaction, arylation, and saponification to complete the synthesis of compound **34**.

In summary, a new class of 2-amino-pyrazine LDHA inhibitors was identified via biochemical screening and validated using biochemical and biophysical assays. The crystal structure of an improved inhibitor indicated that the molecules bind in the active site in the presence of NADH and interact with one of the major catalytic residues involved in substrate catalysis. Structural modifications of the original hit improved the biochemical potency and ligand-efficiency, while also improving the DMPK properties of the compounds. Additional efforts to obtain potent and cell-active LDHA inhibitors will be reported in due course.



Scheme 1. Reagents and conditions: (a) (*R*)-methyl-benzylamine, *N,N*-diisopropylethylamine, *n*-BuOH, M.W. 150 °C, 6 h, 86% yield; (b) Pd(dppf)Cl₂ (10 mol %), ArB(OH)₂ or ArB(pin), Cs₂CO₃, 1,4-dioxane, water, M.W. 120 °C, 30 min, 5–20% yield; (c) ethyl 1*H*-pyrazole-4-carboxylate, CuI (10 mol %), *N*¹,*N*²-dimethylethane-1,2-diamine (20 mol %), Cs₂CO₃, 1,4-dioxane, reflux, 1 h, 39% yield; (d) LiOH, MeOH, water, 23–60 °C, 12 h, 5–40% yield; (e) primary or secondary amine, *N,N*-diisopropylethylamine, *n*-BuOH, reflux, 1 h, 60% yield; (f) NaH, (*R*)-1-phenylethanol, THF, 0 °C → reflux, 2 h, 16% yield.



Scheme 2. Reagents and conditions: (a) (1-bromoethyl)benzene, EtOH, reflux, 18 h, 7% yield; (b) Pd(dppf)Cl₂ (10 mol %), 3-(ethoxycarbonyl)phenylboronic acid, Cs₂CO₃, 1,4-dioxane, water, reflux, 1 h, 5–32% yield; (c) LiOH, MeOH, water, 23 °C, 12 h, 5–40% yield; (d) (*R*)-methyl-benzylamine, triethylamine, EtOH, 23 °C, 12 h, 41% yield; (e) Pd/C (10 mol %), H₂ (1 atm), EtOH, 23 °C, 18 h, 50% yield; (f) (*R*)-methyl-benzylamine, *N,N*-diisopropylethylamine, *n*-BuOH, reflux, 1 h, 60% yield; (g) 37% formalin, AcOH, NaBH(OAc)₃, 23 °C, 12 h, 45% yield; (h) Ac₂O, ZnCl₂ (10 mol %), 23 °C, 2 h, 80% yield; (i) MeSO₂Cl, pyridine, 23 °C, 0.5 h, 30% yield; (j) *N*-bromosuccinimide, benzoylperoxide (1 mol %), CCl₄, 23 °C, 2 h, 28% yield.

Acknowledgements

We thank Drs. Krista Bowman and Jian sheng Wu and their respective Genentech research groups for performing protein expression and purification activities. We also thank Dr. Peter Jackson for many helpful discussions regarding LDHA. In addition, we thank Dr. Patrick Lupardus and Crystallographic Consulting, LLC for diffraction data collection. The Advanced Light Source is supported by the Director, Office of Science, Office of Basic Energy Sciences, of the U.S. Department of Energy under Contract No. DE-AC02-05CH11231.

Supplementary data

Supplementary data associated with this article can be found, in the online version, at <http://dx.doi.org/10.1016/j.bmcl.2013.08.060>.

References and notes

1. Warburg, O. *Science* **1956**, *123*, 309.
2. Vander Heiden, M. G.; Cantley, L. C.; Thompson, C. B. *Science* **2009**, *324*, 1029.
3. (a) Vander Heiden, M. G. *Nat. Rev. Drug Disc.* **2011**, *10*, 671; (b) Tennant, D. A.; Durán, R. V.; Gottlieb, E. *Nat. Rev. Cancer* **2010**, *10*, 267.
4. Ward, P. S.; Thompson, C. B. *Cancer Cell* **2012**, *21*, 297.
5. (a) Balinsky, D.; Platz, C. E.; Lewis, J. W. *Cancer Res.* **1983**, *43*, 5895; (b) Goldman, R. D.; Kaplan, N. O. *Cancer Res.* **1964**, *24*, 389.
6. Fantin, V. R.; St-Pierre, J.; Leder, P. *Cancer Cell* **2006**, *9*, 425.
7. (a) Kanno, T.; Sudo, K.; Maekawa, M.; Nishimura, Y.; Ukita, M.; Fukutake, K. *Clin. Chim. Acta* **1988**, *173*, 89; (b) Kanno, T.; Sudo, K.; Takeuchi, I.; Kanda, S.; Honda, N.; Nishimura, Y.; Oyama, K. *Clin. Chim. Acta* **1980**, *108*, 267.
8. Granchi, C.; Bertini, S.; Macchia, M.; Minutolo, F. *Curr. Med. Chem.* **2010**, *17*, 672.
9. Le, A.; Cooper, C. R.; Gouw, A. M.; Dinavahi, R.; Maitra, A.; Deck, L. M.; Royer, R. E.; Vander Jagt, D. L.; Semenza, G. L.; Dang, C. V. *Proc. Natl. Acad. Sci.* **2010**, *107*, 2037.
10. Kohlmann, A.; Zech, S. G.; Li, F.; Zhou, T.; Squillace, R. M.; Commodore, L.; Lu, M. T.; Greenfield, X.; Miller, D. P.; Huang, W.-S.; Qi, J.; Thomas, R. M.; Wang, Y.; Zhang, S.; Dodd, R.; Liu, S.; Xu, R.; Xu, Y.; Miret, J. J.; Rivera, V.; Clarkson, T.; Shakespeare, W. C.; Zhu, X.; Dalgarno, D. C. *J. Med. Chem.* **2013**, *56*, 1023.
11. Ward, R. A.; Brassington, C.; Breeze, A. L.; Caputo, A.; Critchlow, S.; Davies, G.; Goodwin, L.; Hassall, G.; Greenwood, R.; Holdgate, G. A.; Mrosek, M.; Norman, R. A.; Pearson, S.; Tart, J.; Tucker, J. A.; Vogtherr, M.; Whittaker, D.; Wingfield, J.; Winter, J.; Hudson, K. *J. Med. Chem.* **2012**, *55*, 3285.
12. (a) Billiard, J.; Annan, R.; Ariazi, J.; Briand, J.; Brown, K.; Campobasso, N.; Chakravorty, S.; Chai, D. Colón, M.; Davenport, E.; Dennison, J.B.; Dodson, C.S.; Gaul, N.J.; Gilbert, S.; Jurewicz, A.J.; Lu, H.; McNulty, D.; McSurdy-Freed, J.; Miller, L.; Nurse, K.; Nuthulaganti, P.R.; Quinn, C.; Schneck, J.L.; Scott, G.F.; Shaw, T.N.; Sherik, C.; Smallwood, A.M.; Sweitzer, S.; Villa, J.P.; Waitt, G.; Wooster, P.F.; Duffy, K. J. *American Association for Cancer Research 104th Annual Meeting*, Washington, DC, April 6–10, **2013**, Book of Abstracts.; (b) Chai, D. Colon, M.; Dodson, C.; Duffy, K.J.; Shaw, A.N. WO2012/061557.; (c) Brown, K.K.; Chai, D.; Dodson, C.S.; Duffy, K.J.; Shaw, A.N. WO2013/096151.; (d) Brown, K.K.; Chai, D.; Dodson, C.S.; Duffy, K.J.; Shaw, A.N. WO2013/096153.
13. (a) Granchi, C.; Roy, S.; Giacomelli, C.; Macchia, M.; Tuccinardi, T.; Martinelli, A.; Lanza, M.; Betti, L.; Giannicini, G.; Lucacchini, A.; Funel, N.; León, L. G.; Giovannetti, E.; Peters, G. J.; Palchadhuri, R.; Calvaresi, E. C.; Hergenrother, P. J.; Minutolo, F. *J. Med. Chem.* **2011**, *54*, 1599; (b) Granchi, C.; Roy, S. De.; Simone, A.; Salvetti, I.; Tuccinardi, T.; Martinelli, A.; Macchia, M.; Lanza, M.; Betti, L.; Giannicini, G.; Lucacchini, A.; Giovannetti, E.; Sciarillo, R.; Peters, G. J.; Minutolo, F. *Eur. J. Med. Chem.* **2011**, *46*, 5398.
14. Dragovich, P. S.; Fauber, B. P.; Corson, L. B.; Ding, C. Z.; Eigenbrot, C.; Ge, H.; Giannetti, A. M.; Hunsaker, T.; Labadie, S.; Liu, Y.; Malek, S.; Pan, B.; Peterson, D.; Pitts, K.; Purkey, H. E.; Sideris, S.; Ultsch, M.; VanderPorten, E.; Wei, B.; Xu, Q.; Yen, I.; Yue, Q.; Zhang, H.; Zhang, X. *Bioorg. Med. Chem. Lett.* **2013**, *23*, 3186.
15. The standard error of the mean for reference compounds in the LDHA biochemical assay was $\pm 50\%$. For more details, see: Vander Porten, E.; Frick, L.; Turincio, R.; Thana, P.; La Marr, W.; Liu, Y. *Anal. Biochem.*, in press, dx.doi.org/10.1016/j.ab.2013.07.003.
16. See the [Supplementary data](#) section for details regarding the enzyme, SPR, and cell assay methods.
17. Hopkins, A. L.; Groom, C. R.; Alex, A. *Drug Discovery Today* **2004**, *9*, 430.
18. LDHA preferentially catalyses the formation of lactate from pyruvate, whereas LDHB preferentially catalyzes the reverse reaction. LDHA and LDHB share high levels of binding site homology—all of the key catalytic residues are conserved. Overall, the two enzymes share 83% homology when compared via sequence alignment (see Ref. 11 for additional details).
19. NADH binding to LDHA prior to the binding of pyruvate is the accepted LDHA catalytic mechanism. See Ref. 8 for additional details.
20. Kalgutkar, A. S.; Daniels, J. S. *Carboxylic Acids and Their Bioisosteres*. In *Metabolism, Pharmacokinetics and Toxicity of Functional Groups*; Smith, D. A., Ed., 1st ed.; The Royal Society of Chemistry: Cambridge, 2010; pp 126–143.
21. No attempts were made to identify which, if any, pyrazinone tautomer dominated in organic and/or aqueous solutions. Compound **30** is arbitrarily drawn and described as the phenolic tautomer.
22. See the [Supplementary data](#) for experimental details associated with the described co-crystal structure. All crystallographic descriptions are based on analysis of the ligand chain 'W'/protein chain 'D' LDHA protomer. Two other LDHA protomers containing bound ligand were also observed in the tetramer asymmetric unit. The protein–ligand interactions noted in these other protomers were similar to those described for the ligand chain 'W'/protein chain 'D' complex, although some subtle differences were apparent. See the deposited PDB file for additional structural details: 4M49.
23. The LDHA residue numbering scheme used herein follows the convention of PDB entries 1I10 and 4AJP which does not account for the initiating methionine in the gene sequence reflected in UniProt entry P00338. This numbering scheme differs by one residue from that described elsewhere: Chung, F. Z.; Tujibo, H.; Bhattacharyya, U.; Sharief, F. S.; Li, S. S. *Biochem. J.* **1985**, *231*, 537.
24. For other examples of lactate dehydrogenase crystal structures containing NADH, see: (a) Chaikwad, A.; Fairweather, V.; Conners, R.; Joseph-Horne, T.; Turgut-Balik, D.; Brady, R. L. *Biochemistry* **2005**, *44*, 16221; (b) Read, J. A.; Winter, V. J.; Eszes, C. M.; Sessions, R. B.; Brady, R. L. *Proteins* **2001**, *43*, 175.
25. Human LDHA and human MDH2 protein sequences share 20% similarity. X-ray structures of their protomers can be superimposed using 173 pairs of C α atoms with an rms deviation of 1.7 Å. C α atoms within 5 Å of bound NADH can be superimposed with an rms deviation of 0.7 Å.
26. Cui, J. J.; Tran-Dubé, M.; Shen, H.; Nambu, M.; Kung, P.-P.; Pairish, M.; Jia, L.; Meng, J.; Funk, L.; Botrous, I.; McTigue, M.; Grodsky, N.; Ryan, K.; Padriue, E.; Alton, G.; Timofeevski, S.; Yamazaki, S.; Li, Q.; Zou, H.; Christensen, J.; Mroczkowski, B.; Bender, S.; Kania, R. S.; Edwards, M. P. *J. Med. Chem.* **2011**, *54*, 6342.
27. Irvine, J. D.; Takahashi, L.; Lockhart, K.; Cheong, J.; Tolan, J. W.; Selick, H. E.; Grove, J. R. *J. Pharm. Sci.* **1999**, *88*, 28.
28. CYP in vitro assay panel included the following isoforms: CYP3A4, CYP2C9, CYP2D6, CYP2C19, and CYP1A2.
29. (a) Zimmermann, P. J.; Brehm, C.; Buhr, W.; Palmer, A. M.; Volz, J.; Simon, W.-A. *Bioorg. Med. Chem.* **2008**, *16*, 536; (b) Sevilla, S.; Fornis, P.; de la Fernández, J.-C.; Figuera, N.; Eastwood, P.; Albericio, F. *Tetrahedron Lett.* **2006**, *47*, 8603.
30. Miyaura, N. *Mechanistic Aspects of Metal-Catalyzed Cross-Coupling Reactions of Organoboron Compounds with Organic Halides*. In *Metal-Catalyzed Cross-Coupling Reactions*; de Meijere, A.; Diederich, F., Eds., 2nd ed.; Wiley-VCH Verlag GmbH & Co. KGaA: Weinheim, 2004; Vol. 1, pp 41–123.
31. Jiang, L.; Buchwald, S. *Palladium-Catalyzed Aromatic Carbon–Nitrogen Bond Formation*. In *Metal-Catalyzed Cross-Coupling Reactions*; de Meijere, A.; Diederich, F., Eds., 2nd ed.; Wiley-VCH Verlag GmbH & Co. KGaA: Weinheim, 2004; Vol. 2, pp 699–760.
32. Liu, Y.; Zhang, W.; Sayre, L. M. *J. Heterocycl. Chem.* **2010**, *47*, 683.
33. Chianelli, D.; Molteni, V.; Albaugh, P.A.; Choi, H.-S.; Loren, J.; Wang, Z.; Mishra, P. WO 2010/127152.
34. Mori, K.; Maki, S.; Niwa, H.; Ikeda, H.; Hirano, T. *Tetrahedron* **2006**, *62*, 6272.